Nonlinear optical microscopy: use of second harmonic generation and two-photon microscopy for automated quantitative liver fibrosis studies

Nonlinear optical microscopy: use of second harmonic generation and two-photon microscopy for automated quantitative liver fibrosis studies

Wanxin Sun*
Institute of Bioengineering and Nanotechnology
The Nanos #4-01
31 Biopolis Way
Singapore, Singapore 138669

Shi Chang*
Central-South University
Xiangya Hospital
Department of General Surgery
Changsha, Hunan 410008, China
and
National University of Singapore
Department of Physiology
MD9, 2 Medical Drive
Singapore, Singapore 117597

Dean C. S. Tai
Institute of Bioengineering and Nanotechnology
The Nanos #4-01
31 Biopolis Way
Singapore, Singapore 138669

Nancy Tan
National University of Singapore
Department of Physiology
MD9, 2 Medical Drive
Singapore, Singapore 117597
and
K. K. Women's and Children's Hospital
Department of Paediatrics
100 Bukit Timah Road
Singapore, Singapore 229899

Guangfa Xiao
Central-South University
Xiangya Hospital
Department of General Surgery
Changsha, Hunan 410008, China
and
National University of Singapore
Department of Physiology
MD9, 2 Medical Drive
Singapore, Singapore 117597

Huihuan Tang
Central-South University
Xiangya Hospital
Department of General Surgery
Changsha, Hunan 410008, China

Hanry Yu
Institute of Bioengineering and Nanotechnology
The Nanos #4-01
31 Biopolis Way
Singapore, Singapore 138669
and
National University of Singapore
Department of Physiology and Graduate Programme in Bioengineering
Graduate School for Integrative Science and Engineering and Tissue-Engineering Programme
DSO Labs
Singapore, Singapore 117597
and
Singapore-MIT Alliance
E4-04-10, 4 Engineering Drive 3
Singapore, Singapore 117576
and
Massachusetts Institute of Technology
Department of Mechanical Engineering
Cambridge, Massachusetts 02139

Abstract. Liver fibrosis is associated with an abnormal increase in an extracellular matrix in chronic liver diseases. Quantitative characterization of fibrillar collagen in intact tissue is essential for both fibrosis studies and clinical applications. Commonly used methods, histological staining followed by either semiquantitative or computerized image analysis, have limited sensitivity, accuracy, and operator-dependent variations. The fibrillar collagen in sinusoids of normal livers could be observed through second-harmonic generation (SHG) microscopy. The two-photon excited fluorescence (TPEF) images, recorded simultaneously with SHG, clearly revealed the hepatocyte morphology. We have systematically optimized the parameters for the quantitative SHG/TPEF imaging of liver tissue and developed fully automated image analysis algorithms to extract the information of collagen changes and cell necrosis. Subtle changes in the distribution and amount of collagen and cell morphology are quantitatively characterized in SHG/TPEF images. By comparing to traditional staining, such as Masson's trichrome and Sirius red, SHG/TPEF is a sensitive quantitative tool for automated collagen characterization in liver tissue. Our system allows for enhanced detection and quantification of sinusoidal collagen fibers in fibrosis research and clinical diagnostics. [DOI: 10.1117/1.3041159]

Keywords: second harmonic generation; two-photon excited fluorescence; liver fibrosis; fibrillar collagen; quantification.

Paper 08095R received Mar. 21, 2008; revised manuscript received Jul. 18, 2008; accepted for publication Aug. 28, 2008; published online Dec. 15, 2008.

1 Introduction

Liver fibrosis is associated with the excessive deposition of extracellular matrix (ECM) proteins, such as collagen, as a recurrent wound healing responses to most chronic liver diseases.[1] The abnormal increase in collagen fibers causes the

*Contributed equally as first authors.

Address all correspondence to: Dean C. S. Tai, Institute of Bioengineering and Nanotechnology, The Nanos #4-01, 31 Biopolis Way, Singapore 138669; Tel: (65)68247191; Fax: (65)64789080; E-mail: dtai@ibn.a-star.edu.sg.

1083-3668/2008/13(6)/064010/7/$25.00 © 2008 SPIE

derangement of liver architecture, hampers intrahepatic blood flow, and subsequently causes persistent and progressive hepatic dysfunction.[2] The degree of liver fibrosis is a key indicator for staging and grading chronic liver diseases and for therapeutic efficacy evaluation.[3–6] Therefore, assessing collagen content in livers accurately and objectively is extremely important in both research and clinical context.[3,6–8]

Grading of liver fibrosis is performed with descriptive or semiquantitative scoring systems using stained liver tissues.[3–8] These methods focus on the qualitative rather than quantitative properties of fibrosis development, and results are highly subjected to interpretations by the observers.[9–13] It is difficult to provide a highly reproducible and standardized scoring system for diagnostic purposes.[2] The intra- and interobserver discrepancy is as high as 35% in the assessment of liver fibrosis[9,14–17] despite efforts to improve diagnostic accuracy for qualitative scoring systems.[4,7] These scoring systems remain rough classifications of the severity of fibrosis.[4]

Digital morphometric image analysis has been attempted to quantify liver fibrosis.[2,5,11,12,18,19] A decrease of collagen after treatment was observed in cases where conventional descriptive histology scoring failed to show any significant changes.[20] Operator-input parameters are still required for features such as thresholding and segmentation, giving rise to interassay differences that bias the reproducibility and objectivity of quantifications.[12] Here, we aim to develop a highly objective and reproducible automated image-based liver fibrosis quantification system.[12,19,21,22]

Recent developments in both mode-locked lasers and highly sensitive optical sensors have made nonlinear optical microscopy, such as the multiphoton excited fluorescence[23,24] and multiharmonic generation,[25,26] an affordable option for tissue imaging. Second-harmonic generation (SHG) microscopy is used to measure highly ordered structures without central symmetry in tissue, such as type 1 collagen.[27,28] Being a nonabsorption process that causes no photochemical damage to specimens, SHG is ideal for tissue imaging.

We combined two-photon excited fluorescence (TPEF) and SHG microscopes and systematically optimized the parameters for sensitive and quantitative imaging of liver fibrosis. Fully automated quantification algorithms were developed to assess liver fibrosis progression and cell necrosis. Collagen is further classified into two groups: fine collagen distributed in sinusoidal regions (distributed collagen) and the large patches located in the portal tracts in the region of the blood vessels and bile ducts (aggregated collagen), to study redistribution between these two patterns of collagen in the early stages of liver fibrosis.

2 Methods

2.1 *Animal and Patient Samples*

All procedures were performed on male Wistar rats, with initial weight of 90–100 g. Animals were housed in the Animal Holding Unit of the National University of Singapore (NUS) with free access to lab chow and water in a 12:12-h light/dark schedule. Experiments were approved by the Institutional Animal Care and Use Committee. Human liver samples were obtained from Xiang Ya Hospital in China with approval from the ethics committee of Xiang Ya Hospital.

Intraperitoneal injection of a 1:1 mixture of carbon tetrachloride (CCl_4) with vegetable oil was administered three times a week at a dose of 0.1 mL/100 g, for up to three weeks, according to an established protocol for inducing liver fibrosis.[29,30] Tissues were harvested on days 3, 14, and 21 ($n=3$ per group) under sodium pentobarbital. Cardiac perfusion with 4% paraformaldehyde was performed to flush out blood cells and fix the liver tissue before harvesting. Liver specimens were taken for both cryopreservation and conventional paraffin sections. Cryosections were processed at a thickness of 50 μm while paraffin blocks were cut to a thickness of 4 μm. Human biopsy samples (three patients) were fixed in buffered formalin, embedded in paraffin, and sectioned at 4 μm in thickness.

2.2 *Imaging System*

The nonlinear optical microscope was developed based on a confocal imaging system (LSM 510, Carl Zeiss) using an external tunable mode-locked Ti:sapphire laser (Mai-Tai broadband, Spectra-Physics). The laser was routed to an acousto-optic modulator (AOM) for power attenuation, then through a dichroic mirror (490 nm) and an objective lens to the tissue sample [Fig. 1(a)]. TPEF emission generated in tissue was collected by the same objective lens and recorded by a photomultiplier tube (PMT), after passing through the dichroic mirror and a 700-nm short-pass filter. SHG signal was collected using a high numerical aperture (NA) condenser and a field diaphragm, and was filtered by a 450-nm bandpass filter (10-nm bandwidth) before entering PMT (Hamamatsu R6357) for detection. Note that, with the intrinsic optical sectioning characteristics for nonlinear optical process, the pinhole function of the confocal microscope was not used.

2.3 *Imaging Acquisition*

Samples were initially imaged using SHG/TPEF microscopy, where tissue staining was not required. Two to three images (4096×4096 pixels with dimensions 3.68×3.68 mm) were scanned for each tissue slice, depending on sample size.

Tissue samples were divided into two groups: one stained with Sirius red (Fluka No. 43556) and then imaged with conventional confocal microscope, while the other group was stained with Masson's trichrome (Sigma-Aldrich No. HT15, No. HT101128, and No. HT1079), and imaged by a 5-M-pixel digital camera (MicroPublisher 5.0 RTV, QImaging).

2.4 *Quantification of Distributed and Aggregated Collagen*

One great advantage of SHG microscopy over conventional histological imaging is the ability to monitor collagen formation and remodeling in early fibrosis stages. In order to detect subtle changes, we differentiated collagens into distributed and aggregated collagens using the following algorithm: background in raw SHG images was removed by subtracting a prerecorded background image, and then images were low-pass filtered for three times successively. Filtering was implemented in frequency domain rather than using a traditional convolution method for simplicity and fast processing. Subsequently, Otsu threshold segmentation was applied[31] to create a binary map as a mask (detailed image processing algorithm is

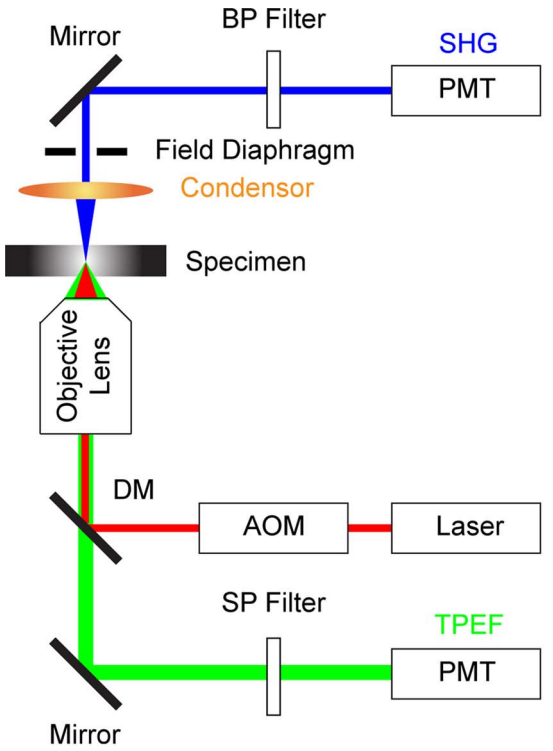

Fig. 1 (a) Schematic illustration of the optical configuration: Excitation laser was a tunable mode-locked laser (710–990 nm) with an AOM for power control. The laser went through a DM (490 nm), an objective lens, and reached tissue specimen. An SHG signal was collected on the opposite side the laser source, by a high NA condenser, through a field diaphragm and a 450-nm band-pass (BP) filter, before being recorded by a PMT. TPEF was collected by the objective lens, filtered by a 700-nm short-pass (SP) filter before being recorded by another PMT. (b) Dependence of SHG signal intensity on NA of the objective lens, NA of the condenser, and the thickness of liver slices. For thin tissue samples, thickness=150 μm, SHG signal intensity reached a plateau when NA of the condenser roughly equals to the NA of objective lens. However, for thick slices (~300 μm), SHG signal continued to increase even when the condenser NA is larger than the objective NA.

available on request). We then multiplied this mask to the original SHG image, in which background noise was removed by subtracting the prerecorded background image. Residual grainy noise was removed by using erosion and dilation functions.[32] During this procedure, only large collagen colonies with high connectivity (aggregated collagen) were retained in the end, while distributed collagen was set to zero. Finally, distributed collagen was identified by subtracting aggregated collagen from the original SHG image. The average intensity value of all the pixels was measured where collagen was present.

2.5 *Quantitative Analysis of Cell Necrosis*

During fibrosis induction, some hepatocytes degenerated and formed dark regions in TPEF images. To quantitatively describe this process, the TPEF images were processed using the following algorithm: background and grainy noises were removed (similar to the previous algorithm), followed by a low-pass filter to further suppress noise. Finally, Otsu threshold segmentation was applied to create a binary map. All the objects (dark areas) were identified in the image. The area and aspect ratio for each of these objects were calculated. If the area of an object was smaller than a critical value, α (preselected as the area of a single hepatocyte), then this object was classified as sinusoidal space. For the objects with area greater than α, normalized area (area divided by aspect ratio) would then be calculated. If the normalized area was larger than a critical value β (preselected as the normalized area of a single hepatocyte), then these objects would be classified as blood vessels because blood vessels are generally larger and more regular (circular) in shape than a single hepatocyte. After identification of sinusoidal spaces and blood vessels, the rest of the objects were classified as cell damage areas. Once these three objects were categorized, the area of cell necrosis was calculated by summing the cell damage areas after the exclusion of blood vessels and sinusoidal spaces (detailed image processing algorithm is available on request).

3 Results

3.1 *Design and Optimization of SHG Detection System*

The sensitivity of the detection and light collection efficiency of the SHG system was optimized to obtain the best images for further analysis. In particular, a combination of condenser NA and the thickness of the liver slices were characterized systematically to obtain the highest SHG signal. Figure 1(b) illustrates that SHG signal intensity increases as the condenser NA increases. For thin slices (150 μm), SHG signal intensity reaches a plateau when the condenser NA roughly equaled to that of the objective lens. This observation is similar to that reported by Moreaux et al.,[33,34] in membranes, where most of the SHG would be collected if the SHG emission pattern is confined and the collection NA is equal to the excitation NA. For thick slices (300 μm), the SHG signal continues to increase even when the condenser NA is larger than the objective NA. The scattering in thick tissues is severe such that SHG signals are strong enough to be recorded in the backward direction, although these signals are generally weaker than the forward SHG signals.

In order to maximize SHG signal collection efficiency, NA of 0.8 was chosen for the condenser while NA for the dry objective lenses were typically <0.7 in our settings. Further increase in condenser NA did not improve the collection efficiency significantly [Fig. 1(b)] because scattering of SHG sig-

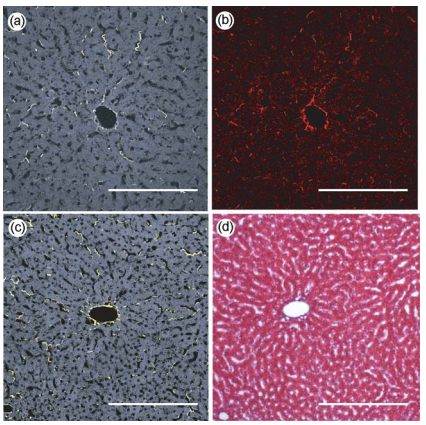

Fig. 2 Images of collagen fibers in liver tissue slices: (a) Superposition of SHG and TPEF image of a normal liver slice and (b) the confocal fluorescence image of the same liver sample shown in (a) after staining with Sirius red. Sirius red stained all collagen fibers in tissue and confirmed that SHG detects the presence of collagen faithfully. (c) SHG/TPEF image of another normal liver slice and (d) a bright-field transmission image of the same tissue sample in (c), stained with Manson's trichrome. Collagen around the vessel wall appeared blue as expected with Manson's trichrome staining, while collagen in the sinusoid was too fine to be identified in these images. TPEF is shown in dark gray; SHG is in gold and the scale bars shown are 200 μm. (Color online only.)

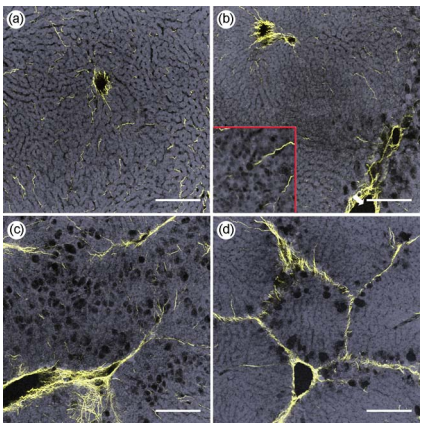

Fig. 3 Morphological changes at different stages of liver fibrosis recorded with SHG and TPEF microscopies: (a) Collagen fibers were uniformly distributed throughout the normal liver slice, and no necrosis (dark region) was observed in TPEF image. (b) Hepatocyte balloon degeneration appeared around the central vein (pointed by the white arrow) three days after CCl_4 injection. Development of necrosis (dark areas) started at this stage, which could be seen in the magnified view at the bottom left corner. In addition, the amount of distributed collagen fibers appeared to be decreasing as well. (c) Vacuoles caused by hepatocyte necrosis appear massively, and collagen tended to form septa after continuous injection of CCl_4 for 14 days. (d) Bridge fibrosis was formed after injection for 21 days. TPEF is shown in dark gray, SHG is in gold, and the scale bars shown are 200 μm. (Color online only.)

nal in tissue made it similar to that generated from a much more diffused spot. This was validated with Monte Carlo simulation (data not shown). In addition, liver tissue exhibits much higher autofluorescence in comparison to other organs, such as kidney;[27] and this presents a great technical challenge to image and quantify fibrosis progression in livers. In our system, we incorporated a field diaphragm as a spatial filter to suppress noise and background stray light, and hence obtaining an improved signal level in the SHG detection.

3.2 *Comparison between SHG/TPEF and Conventional Histological Imaging*

Despite high interassay differences during staining that leads to low reproducibility and lack of objectivity for quantifications, Sirius red is still commonly used for routine assessment of liver fibrosis.[12] To verify that SHG/TPEF microscopy (excitation wavelength=900 nm) is detecting only collagen, we compared the SHG/TPEF results to that obtained with Sirius red staining [excitation wavelength=543 nm, built-in He–Ne laser; Figs. 2(a) and 2(b) respectively]. Features observed in the SHG/TPEF image also appear in the Sirius red fluorescence image, confirming that the SHG signals reflect fibrillar collagen faithfully.

We further compared our results to images acquired with Masson's trichrome staining [Figs. 2(c) and 2(d)], which is the gold standard in a typical pathology laboratory for clinical diagnosis of liver fibrosis.[35] Unlike Sirius red, Masson's trichrome targets ECM, in general, including collagen. The fiber stain component of this tricolored process yields a variable, wide blue-green spectrum. One particular challenge lies in producing uniform interbatch shades of the three colors involved and selecting the green or blue shade for analysis, resulting in nonreproducible results when used as a quantitative measure of fibrosis progression. Both methods clearly demonstrated collagen aggregation around vessel walls; however, only SHG images showed collagen fibers inside the sinusoids. Therefore, SHG microscopy can yield sensitive and quantitative information about collagen in liver tissues.

3.3 *Liver Fibrosis Progression*

SHG and TPEF microscopies were used to simultaneously quantify changes in fibrillar collagen and the hepatocyte morphology during liver fibrosis progression. Excited with a femtopulsed laser, intrinsic molecules in hepatocyte, such as NAD(P)H and flavins, emitted substantial fluorescence, making TPEF suitable for cell morphology observation.[36] Areas containing nucleus, lipid droplets, and the vacuoles formed by degenerated hepatocytes appeared dark in the TPEF image due to the lack of the fluorescent molecules. Figure 3 shows changes in collagen (gold color) and cell morphology (gray color) during fibrosis progression. In normal livers [Fig. 3(a)], hepatocytes are healthy and collagen is distributed evenly in sinusoidal spaces. As liver damage progresses, different pathologies can result in different morphologies of collagen distribution during fibrosis. Collagen deposition often starts around the portal region, and as it increases, it eventually "bridges" and connects to form nodules in advanced fibrosis, with resultant liver cirrhosis. Three days after intraperitoneal injection of CCl_4, hepatocyte degeneration and microvesicular fatty changes around the central vein can be observed [Fig. 3(b)]. By day 14, accumulation of the fibrillar collagen appears around the necrotic areas and thin fibrous septae are formed with centrilobular bridging [Fig. 3(c)]. By day 21, collagen fibers form complete bridging [Fig. 3(d)]. Pathological development of liver fibrosis, including subtle changes in

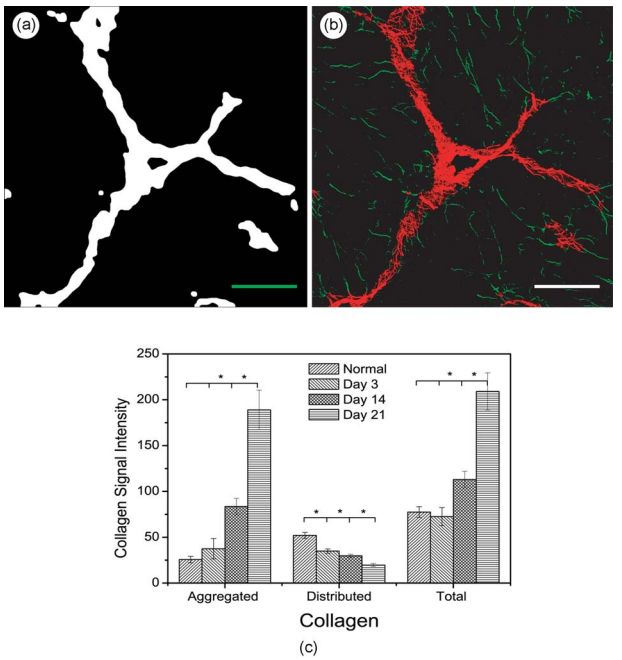

Fig. 4 Identification and quantification of distributed and aggregated collagens: (a) A mask image generated by using low-pass filtering and segmentation from typical collagen images, captured with SHG microscopy. (b) Differentiation results between distributed (green) and aggregated (red) collagen. See text for details on algorithm utilized in this procedure. (c) Graph of collage progression for both collagen types at various time points. It was shown that the distributed collagen fibers decreased significantly from as early as day 3, whereas aggregated collagen only showed slight increase in the first three days. This finding suggested a remodeling between distributed and aggregated collagens during this period. Note that the asterisk in the graph, indicates that the differences reached statistical significance, and the scale bars shown are 200 μm. (Color online only.)

both collagen fibers and hepatocyte morphology, can be clearly recorded by SHG/TPEF imaging. These subtle changes will provide valuable information when studying the severity of liver fibrosis, especially in early stages, as well as to monitor fibrosis resolution after surgical or drug treatment.

3.4 *Quantitative Analysis of Liver Fibrosis Progression*

The amount of collagen in liver tissue is a direct indicator of the severity of fibrosis but has not been used as a parameter when categorizing stages of liver fibrosis in current clinical practice because of the difficulty in quantifying collagen distribution without a standardized staining and imaging protocol. Common problems encountered include human operation on staining and imaging, intrinsic photobleaching effect of the dye, and color distortion when acquiring the images. SHG/TPEF microscopy and SHG signals do not suffer from these limitations. The signal level can be quantified in a standardized and absolute manner, providing a more objective and accurate diagnosis for liver fibrosis progression.

We have exploited the SHG signals to study the remodeling of collagen during the early stages of liver fibrosis. Distributed collagen fibers were observed to decrease while the aggregated collagen patches increased with the fibrosis progression (Fig. 3). A mask was generated [Fig. 4(a)] to differentiate aggregated from distributed collagen; and outcomes are illustrated in Fig. 4(b). Distributed and aggregated collagens were quantified separately for all samples, showing a decline in distributed collagen fibers from as early as day 3, whereas an increase in aggregated collagen was observed in the first three days [Fig. 4(c)]. Interestingly, the total amount of collagen (the sum of both distributed and aggregated collagen) did not show a significant increase in the first three days, suggesting that a remodeling from distributed to aggregated collagens may be taking place. This remodeling process was not discovered in the past due to the inability to resolve collagen features with the conventional histological imaging techniques. With the SHG/TPEF system, we can quantitatively measure the severity of liver fibrosis by examining the amount of collage fiber present and study the morphological reformation between distributed and aggregated collagens from the early stages onward.

SHG microscopy also has the advantage of providing insights into the 3-D distributional profile of collagen in tissue samples. In typical SHG images, the area of collagen represents the locations where collagen existed within the optical sectioning layer (x-y plane), while the intensity reflects the amount of collagen in the z direction.[27] We have studied fibrosis progression using both area (data not shown) as well as the averaged intensity of pixels of collagen signals. An identical increasing trend in collagen content was observed as the severity of fibrosis increases in both cases. The variation in total SHG signal intensity seems a better indicator for the 3-D progression of fibrosis because the observed difference in intensity is slightly greater than that using area as a measure. We therefore have chosen average intensity for further data analysis.

3.5 *Quantitative TPEF Imaging of Cell Damage during Liver Fibrosis*

The degeneration and necrosis of hepatocytes result in deterioration of tissue structure and intracellular fluorescent molecules. Representative dark regions were easily identified in the TPEF images [Fig. 5(a)]. Area and aspect ratios were calculated for sinusoidal spaces, cell damage areas, and blood vessels [see Fig. 5(b)]. Classification of blood vessels was further confirmed manually to minimize error. Quantified result of the damage area is plotted in Fig. 5(c) where the damaged areas do not increase as fibrosis progresses, suggesting that liver regeneration might be more significant than the hepatocyte damage caused by CCl_4 between day 14 and day 21 (later stages of fibrosis or cirrhosis).

3.6 *Future Clinical Applications*

We have described a platform for standardized quantification of collagen content in the rat liver tissue and further evaluated the use of the SHG/TPEF system to quantitatively characterize and monitor tissue biopsy samples from human patients suffering from chronic liver disease. SHG images obtained from human samples are shown in Fig. 6. In Fig. 6(a), presence of collagen is observed around the portal area in the biopsy sample, whereas Fig. 6(b) shows a magnified view of Fig. 6(a) around the collagen. The tissue sample shown in

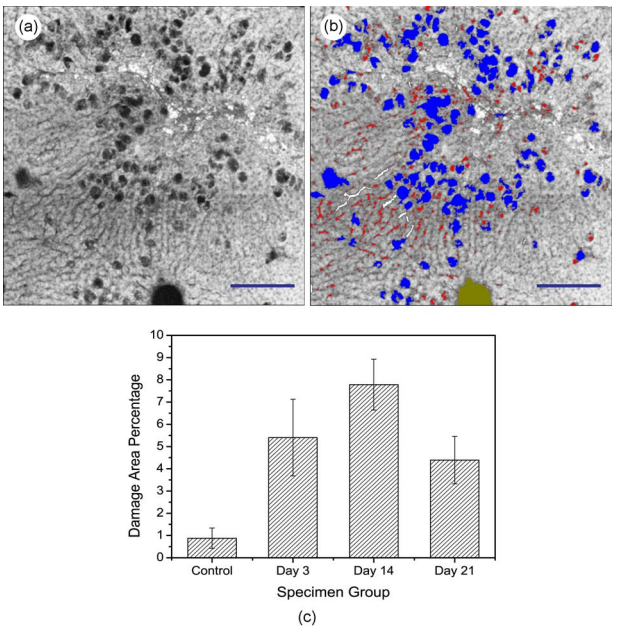

Fig. 5 Quantification of cell damage during fibrosis progression induced by CCl_4 intraperitoneal injection: (a) A TPEF image of fibrotic liver tissue (on day 14); image was smoothed by low-pass filtering and the dark regions represents areas in which cells were damaged. (b) Classification of the objects based on area and aspect ratio, where red and white represented small area and high aspect ratio, respectively; the blood vessel was marked with an olive color, and objects in blue were considered as cell-damage area. Scale bars shown are 200 μm. (c) Quantitative representation of cell damage during the fibrosis progression. The damage area did not increase monotonically due to regeneration mechanism. (Color online only.)

Fig. 6 is a typical example in which collagen could hardly be observed with conventional histology imaging but is clearly identified using SHG microscopy. These observations confirmed that the SHG/TPEF system described in this study presents a potential tool for standardized, time-saving, and accurate liver fibrosis assessment in clinics, especially in the early stages.

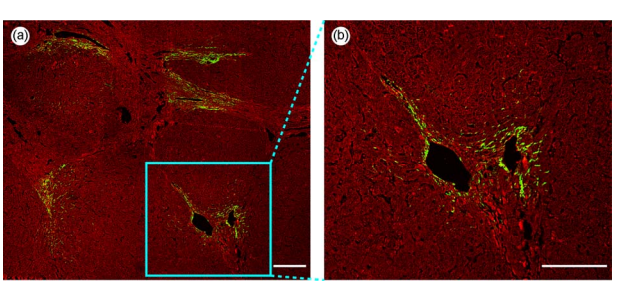

Fig. 6 Superposition of SHG and TPEF images on human patient biopsy samples: (a) Image of a patient specimen, in which collagen fiber could hardly be seen with conventional histological imaging, whereas SHG clearly identified these collagen. (b) Magnified view around the portal area where collagen aggregates; cell morphology and cell damage development (by TPEF) as well as collage distribution can be clearly observed (by SHG). TPEF is shown in red; SHG is shown in green; and the scale bars shown are 200 μm. (Color online only.)

4 Discussion and Conclusion

SHG microscopy has been widely used for imaging collagen fibers in various tissue types and organs.[27,34,37–39] In particular, Banavar et al.,[37] Cox et al.,[38] and Gorrel[39] have validated the feasibility of SHG microscopy for monitoring collagen fiber in fibrotic livers. Similar to our findings, SHG microscopy was demonstrated to measure the presence of collagen more sensitively and accurately than the imaging techniques used in clinical practice.

In current practices, the liver fibrosis assessment involves tissue staining and image acquisition, followed by diagnosis based on morphological features of the tissue sample. The process is tedious and labor intensive, and results suffer from high batch-to-batch variations in staining that lead to high inter- and intraobserver discrepancies in assessments. The use of fluorescent, collagen-specific dyes, such as Sirius red, suffers from intrinsic photobleaching, making it difficult to standardize the quantification process and obtain highly reproducible and quantitative results. Unlike fluorescent processes, SHG signal intensity is not affected by the presence of fluorochromes but is dependent on laser power and NA of the collection optics, which makes results highly quantitative.

In our study, we have developed a comprehensive animal model and successfully recorded livers fibrosis progression in both qualitative and quantitative context. We have further optimized the SHG detection sensitivity and collection efficiency systematically by choosing appropriate parameters like NA and incorporating components such as field diaphragm and condenser. Together with custom-developed image processing algorithms, we could detect and quantify fine collagens distributed in sinusoidal spaces in livers. We have shown the superior sensitivity and spatial resolution of SHG/TPEF method over the currently employed method, where Masson's trichrome staining is used. We have also demonstrated that SHG/TPEF can be used to track hepatocyte degeneration and necrosis in livers as an indicator for tissue regeneration.

In conclusion, we have developed and characterized a standardized quantification mechanism for quantitative measure of liver fibrosis. We have, for the first time, established the spatial classification of the sinusoidal versus portal fibrillar collagen and observed the collagen remodeling that takes place in early stages of liver fibrosis. This opens the door for investigating the role of collagen remodeling during liver fibrosis development in early stages with fine details of fibrosis resolution for potential treatments. The feasibility of applying this method for clinical diagnosis and monitoring was also validated using biopsy specimens from human patients.

Acknowledgments

This work is supported, in part, by the Institute of Bioengineering and Nanotechnology, Biomedical Research Council, Agency for Science, Technology and Research (A*STAR) of Singapore and Grants No. R185-001-045-305; No. R-185-000-135-112 (Ministry of Education), No. R-185-000-099-213 (National Medical Research Council) and Singapore-MIT Alliance Computational and Systems Biology Flagship Project funding to H. Yu. Nancy Tan is supported by the ExxonMobil–NUS Clinician Fellowship Award.

References

1. R. Bataller and D. A. Brenner, "Liver fibrosis," *J. Clin. Invest.* **115**(2), 209–218 (2005).
2. M. Kage, K. Shimamatu, E. Nakashima, M. Kojiro, O. Inoue, and M. Yano, "Long-term evolution of fibrosis from chronic hepatitis to cirrhosis in patients with hepatitis C: Morphometric analysis of repeated biopsies," *J. Hepatol* **25**(4), 1028–1031 (1997).
3. P. Bedossa and T. Poynard, "An algorithm for the grading of activity in chronic hepatitis C: The METAVIR Cooperative Study Group," *J. Hepatol* **24**(2), 289–293 (1996).
4. E. M. Brunt, "Grading and staging the histopathological lesions of chronic hepatitis: The Knodell histology activity index and beyond," *J. Hepatol* **31**(1), 241–246 (2000).
5. G. M. Dahab, M. M. Kheriza, H. M. El-Beltagi, A. M. Fouda, and O. A. El-Din, "Digital quantification of fibrosis in liver biopsy sections: description of a new method by Photoshop software," *J. Gastroenterol. Hepatol* **19**(1), 78–85 (2004).
6. V. J. Desmet, M. Gerber, J. H. Hoofnagle, M. Manns, and P. J. Scheuer, "Classification of chronic hepatitis: diagnosis, grading and staging," *J. Hepatol* **19**(6), 1513–1520 (1994).
7. K. Ishak et al., "Histological grading and staging of chronic hepatitis," *J. Hepatol* **22**(6), 696–699 (1995).
8. R. G. Knodell, K. G. Ishak, W. C. Black, T. S. Chen, R. Craig, N. Kaplowitz, T. W. Kiernan, and J. Wollman, "Formulation and application of a numerical scoring system for assessing histological activity in asymptomatic chronic active hepatitis," *J. Hepatol* **1**(5), 431–435 (1981).
9. P. Bedossa, P. Bioulacsage, P. Callard, M. Chevallier, C. Degott, Y. Deugnier, M. Fabre, M. Reynes, J. J. Voigt, E. S. Zafrani, T. Poynard, and G. Babany, "Intraobserver and interobserver variations in liver biopsy interpretation in patients with chronic hepatitis C: The French METAVIR Cooperative Study Group," *J. Hepatol* **20**(1), 15–20 (1994).
10. P. Bedossa, D. Dargere, and V. Paradis, "Sampling variability of liver fibrosis in chronic hepatitis C," *J. Hepatol* **38**(6), 1449–1457 (2003).
11. A. Y. Hui, C. T. Liew, M. Y. Go, A. M. Chim, H. L. Chan, N. W. Leung, and J. J. Sung, "Quantitative assessment of fibrosis in liver biopsies from patients with chronic hepatitis B," *Liver Int.* **24**(6), 611–618 (2004).
12. M. Masseroli, T. Caballero, F. O'Valle, R. M. Del Moral, A. Perez-Milena, and R. G. Del Moral, "Automatic quantification of liver fibrosis: design and validation of a new image analysis method: Comparison with semi-quantitative indexes of fibrosis," *J. Hepatol* **32**(3), 453–464 (2000).
13. R. D. Soloway, A. H. Baggenstoss, L. J. Schoenfield, and W. H. Summerskill, "Observer error and sampling variability tested in evaluation of hepatitis and cirrhosis by liver biopsy," *Am. J. Dig. Dis.* **16**(12), 1082–1086 (1971).
14. A. Theodossi, A. M. Skene, B. Portmann, R. P. Knill-Jones, R. S. Patrick, R. A. Tate, W. Kealey, K. J. Jarvis, D. J. O'Brian, and R. Williams, "Observer variation in assessment of liver biopsies including analysis by kappa statistics," *Gastroenterology* **79**(2), 232–241 (1980).
15. J. Westin, L. M. Lagging, R. Wejstal, G. Norkrans, and A. P. Dhillon, "Interobserver study of liver histopathology using the Ishak score in patients with chronic hepatitis C virus infection," *Liver (Oxford, U. K.)* **19**(3), 183–187 (1999).
16. A. Theodossi, D. J. Spiegelhalter, J. Jass, J. Firth, M. Dixon, M. Leader, D. A. Levison, R. Lindley, I. Filipe, A. Price, N. A. Shepherd, S. Thomas, and H. Thompson, "Observe variation and discriminatory value of biopsy features in inflammatory dowel-disease," *Gut* **35**(7), 961–968 (1994).
17. K. Gronbaek, P. B. Christensen, S. Hamilton-Dutoit, B. H. Federspiel, E. Hage, O. J. Jensen, and M. Vyberg, "Interobserver variation in interpretation of serial liver biopsies from patients with chronic hepatitis C," *J. Viral Hepat.* **9**(6), 443–449 (2002).
18. M. A. Friedenberg, L. Miller, C. Y. Chung, F. Fleszler, F. L. Banson, R. Thomas, K. P. Swartz, and F. K. Friedenberg, "Simplified method of hepatic fibrosis quantification: design of a new morphometric analysis application," *Liver Int.* **25**(6), 1156–1161 (2005).
19. C. Pilette, M. C. Rousselet, P. Bedossa, D. Chappard, F. Oberti, H. Rifflet, M. Y. Maiga, Y. Gallois, and P. Cales, "Histopathological evaluation of liver fibrosis: Quantitative image analysis vs semi-quantitative scores: Comparison with serum markers," *J. Hepatol* **28**(3), 439–446 (1998).
20. N. Manabe, M. Chevallier, P. Chossegros, X. Causse, S. Guerret, C. Trepo, and J. A. Grimaud, "Interferon-alpha 2b therapy reduces liver fibrosis in chronic non-A, non-B hepatitis: A quantitative histological evaluation," *J. Hepatol* **18**(6), 1344–1349 (1993).
21. T. Caballero, A. Perez-Milena, M. Masseroli, F. O'Valle, F. J. Salmeron, R. M. Del Moral, and G. Sanchez-Salgado, "Liver fibrosis assessment with semiquantitative indexes and image analysis quantification in sustained-responder and non-responder interferon-treated patients with chronic hepatitis C," *J. Hepatol* **34**(5), 740–747 (2001).
22. R. G. Knodell, M. D. Kamal, G. Ishak, W. C. Black, T. S. Chen, R. Craig, N. Kaplowitz, T. W. Kiernan, and J. Wollman, "Formulation and application of a numerical scoring system for assessing histological activity in asymptomatic chronic active hepatitis" *J. Hepatol* **1**(5), 431–435 (1981).
23. W. Denk, J. H. Stricjler, and W. W. Webb, "Two-photon laser scanning fluorescence microscopy," *Science* **248**, 73–76 (1990).
24. S. Maiti, R. M. Williams, J. B. Shear, W. R. Zipfel, and W. W. Webb, "Measuring serotonin distribution in live cells with three-photon excitation," *Science* **275**, 530–532 (1997).
25. I. Freund, M. Deutsch, and A. Sprecher, "Connective tissue polarity," *Biophys. J.* **50**, 693–712 (1986).
26. S.-W. Chu, I.-H. Chen, T.-M. Liu, P. C. Chen, C.-K. Sun, and B.-L. Lin, "Multimodal nonlinear spectral microscopy based on a femtosecond Cr: Forsterite laser," *Opt. Lett.* **26**, 1909–1911 (2001).
27. M. Strupler, A. M. Pena, M. Hernest, P. L. Tharaux, J. L. Martin, E. Beaurepaire, and M. C. Schanne-Klein, "Second harmonic imaging and scoring of collagen in fibrotic tissues," *Opt. Express* **15**(7), 4054–4065 (2007).
28. T. A. Theodossiou, C. Thrasivoulou, C. Ekwobi, and D. L. Becker, "Second harmonic generation confocal microscopy of collagen type I from rat tendon cryosections," *Biophys. J.* **91**(12), 4665–4677 (2006).
29. C. Constandinou, N. Henderson, and J. P. Iredale, "Modeling liver fibrosis in rodents," *Methods Mol. Med.* **117**, 237–250 (2005).
30. H. Tsukamoto, M. Matsuoka, and S. W. French, "Experimental models of hepatic fibrosis: A review," *Semin Liver Dis.* **10**, 56–65 (1990).
31. N. Otsu, "A threshold selection method from gray level histograms," *IEEE Trans. Syst. Man Cybern.* **9**, 62–66 (1979).
32. J. Serra, *Image Analysis and Mathematical Morphology*, Academic Press, New York (1982).
33. L. Moreaux, O. Sandre, S. Charpak, M. Blanchard-Desce, and J. Mertz, "Coherent scattering in multi-harmonic light microscopy," *Biophys. J.* **80**, 1568–1574 (2001).
34. L. Moreaux, O. Sandre, and J. Mertz, "Membrane imaging by second-harmonic generation microscopy," *J. Biomed. Opt.* **17**, 1685–1694 (2000).
35. D. Tretheway, A. Jain, R. LaPoint, R. Sharma, M. Orloff, P. Milot, A. Bozorgzadeh, and C. Ryon, "Should trichrome stain be used on all post-liver transplant biopsies with hepatitis C virus infection to estimate the fibrosis score?," *Liver Transpl Surg.* **14**(5), 695–700 (2008).
36. W. R. Zipfel, R. M. Williams, R. Christie, A. Y. Nikitin, B. T. Hyman, and W. W. Webb, "Live tissue intrinsic emission microscopy using multiphoton-excited native fluorescence and second harmonic generation," *Proc. Natl. Acad. Sci. U.S.A.* **100**(12), 7075–7080 (2003).
37. M. Banavar, E. P. W. Kable, F. Braet, X. M. Wang, M. D. Gorrell, and G. Cox, "Detection of collagen by second harmonic microscopy as a diagnostic tool for liver fibrosis-Art. No. 60891B," *Proc. SPIE* **6089**, B891–B891 (2006).
38. G. Cox, E. Kable, A. Jones, I. K. Fraser, F. Manconi, and M. D. Gorrell, "3-dimensional imaging of collagen using second harmonic generation," *J. Struct. Biol.* **141**(1), 53–62 (2003).
39. M. D. Gorrell, X. M. Wang, M. T. Levy, E. Kable, G. Marinos, G. Cox, and G. W. McCaughan, "Intrahepatic expression of collagen and fibroblast activation protein (FAP) in hepatitis C virus infection," *Dipeptidyl Aminopeptidases Health Dis.* **524**, 235–243 (2003).